Designing for seismic resilience: self-centering steel frames with fuse-post-tensioned bars and viscous dampers

A. S. Tzimas[1], A. D. Dimopoulos[2], V. C. Kamperidis[3] and T. L. Karavasilis[4]

[1, 2, 3, 4] University of Warwick, School of Engineering, Coventry, United Kingdom, T.Karavasilis@warwick.ac.uk

ABSTRACT

Self-centering steel moment resisting frames (SC-MRFs) reduce inelastic deformations and eliminate residual drifts under the design basis earthquake. Existing design procedures for SC-MRFs aim to achieve peak drifts similar to those of conventional steel moment resisting frames. The combination of SC-MRFs with viscous dampers has not been properly assessed and research towards the standardization of SC-MRFs within the framework of the Eurocode 8 is missing. This paper presents a seismic design procedure for SC-MRFs within the framework of Eurocode 8 that: a) defines performance objectives with respect to peak storey drifts and limit states in the post-tensioned (PT) connections; b) use viscous dampers to control drifts; c) adopts a fuse system to avoid brittle failures and eliminate the probability of collapse under the maximum considered earthquake. A prototype building is designed as a SC-MRF with viscous dampers. Nonlinear static and dynamic analyses confirm the minimal-damage performance of the SC-MRF and the validity and simplicity of the proposed seismic design procedure.

INTRODUCTION

Conventional moment resisting frames (MRFs) are designed to sustain significant inelastic deformations in main structural members under the design basis earthquake (DBE) (EC8. 2008), which result in difficult to repair damage, residual drifts, and economic losses related to both structural and non-structural damage. Steel self-centering moment-resisting frames (SC-MRFs) with post-tensioned (PT) connections is a new type of resilient structures, that exhibit softening force-drift behaviour and eliminate inelastic deformations in beams and residual drifts due to gap openings developed at the interfaces between the beams and the columns and pre-tensioning bars which clamp beams to the columns and provide self-centering capability. PT connections use special devices which are activated when gaps open and provide energy dissipation. Existing design procedures for SC-MRFs achieve drifts similar to the conventional MRFs, and so, significant non-structural damage is accepted under the DBE (Garlock et al. 2007, Kim et al. 2008). In addition, the proposed PT connections, may suffer a sudden loss of stiffness and strength when loaded beyond the maximum considered earthquake (MCE) drift (Garlock et al. 20007) or exhibit a ductile ultimate response by forming beam plastic hinges when

loaded beyond the DBE drift (Kim et al. 2008). Standardization of SC-MRFs within the framework of EC8 is missing, while their collapse resistance is unknown. Steel MRFs equipped with passive dampers is another class of resilient structures (Symans et al. 2008). A design procedure and a thorough seismic response assessment for steel SC-MRFs with viscous dampers is missing.

This paper presents a seismic design procedure for steel SC-MRFs and a strategy of combining them with viscous dampers within the framework of EC8. The design procedure defines performance levels with respect to drifts, residual drifts and limit states in the PT connections. A fuse system is inserted in the PT connections to avoid possible brittle failures. Different design cases of a prototype building consisting of SC-MRFs with or without viscous dampers are considered to investigate all possible scenarios, i.e. use of dampers to achieve drifts lower than the EC8 ones; to reduce steel weight without exceeding the EC8 drift; or to reduce steel weight and achieve drifts lower than the EC8 ones. Nonlinear analyses using numerical models able to capture all possible structural limit states up to collapse confirm the minimal-damage behaviour of the SC-MRFs, their outstanding collapse resistance, and the validity of the proposed design procedure.

STRUCTURAL DETAILS OF A PT CONNECTION WITH WHPs

Figure 1(a) shows a SC-MRF using PT connections with web hourglass shape pins (WHPs) and Figure 1(b) shows an exterior PT connection. Two high strength steel bars, located at the mid depth of the beam, one at each side of the beam web, pass through holes drilled on the column flanges. The bars are post tensioned and anchored to the exterior columns. WHPs are inserted in aligned holes on the beam web and on supporting plates welded to the column flanges. The WHPs have an optimized hourglass shape with enhanced fracture capacity (Vasdravellis et al. 2013). The beam web and the beam flanges are reinforced with steel plates. The panel zone is strengthened with doubler and continuity plates. A fin plate with slotted holes, welded on the column flange, is used for easy erection and resistance against gravity loads before post-tensioning. Slotted holes on the fin plate ensure negligible influence of the fin plate on the connection behaviour. To avoid brittle failures in the PT connection due to beam web and flange inelastic buckling or PT bar yielding (seen in experiments and finite element analyses (Vasdravellis et al. 2013, Tzimas et al. 2013, Dimopoulos et al. 2013), the use of a fuse-PT bar mechanism is proposed. A short stocky steel beam (referred to as 'fuse') is welded on a strong plate bolted on the exterior column flange to enable replacement. PT bars are anchored on a stiff plate welded on the fuse. The fuse is designed to yield at a predefined force level to limit the peak force and elongation of the PT bars.

(a)

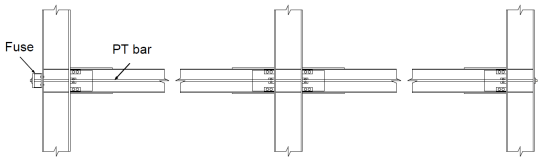

(b)

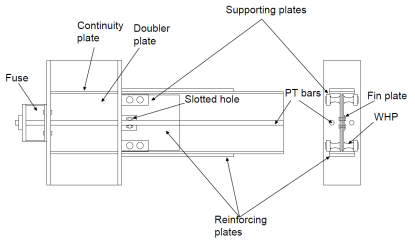

Figure 1. (a) SC-MRF; (b) and exterior PT connection with WHPs

PT CONNECTION BEHAVIOR

The connection is characterized by gap opening and closing in the beam-column interface as a result of the re-centering force in the PT bars. Figure 2(a) shows the free body diagram of an external PT connection where d_{1u} and d_{1l} are the distances of the upper and lower WHPs from the center of rotation (COR) that is assumed to be at the inner edge of the beam flange reinforcing plates; d_2 is the distance of the PT bars from the COR; T is the total force in both PT bars; $F_{WHP,u}$ and $F_{WHP,l}$ are the forces in the upper and lower WHPs; C_F is the compressive force in the beam-column interface; V_{c1u} and V_{c1l} are the shear forces in the upper and lower column, M is the PT connection moment, V is the beam shear force; and N is the horizontal clamping force in the beam-column interface. Figure 2(b) shows the SC-MRF expansion due to rotations θ in the PT connections. The slab inertia forces F_{Dj} are transferred to the mid-depth of the beams of the SC-MRF by secondary beams and are in equilibrium with the column shear forces. Based on Figures 2(a & b), N is given by $N=T+V_{C1u}-V_{C1l}$ for an external and $N=T+\Sigma(V_{C1u}-V_{C1l})+\Sigma F_D$ for an internal connection.

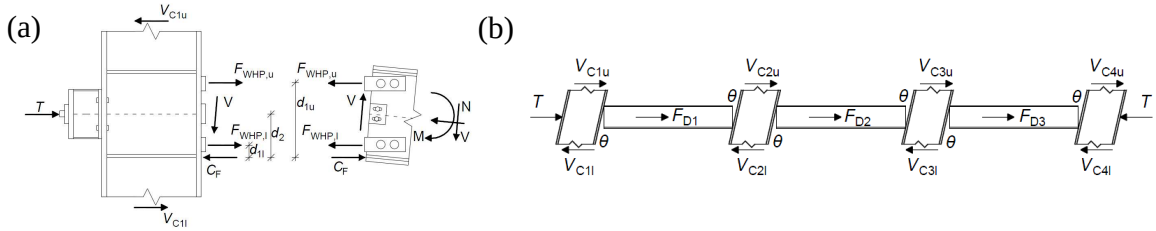

Figure 2. (a) Free body diagram of an external PT connection; and (b) SC-MRF expansion and horizontal forces of equilibrium

Figure 3(a) shows the theoretical cyclic M-θ behaviour of the PT connection with WHPs. M is the summation of M_N and M_{WHP}, where M_N is the moment contribution from N (see Figure 3(b)) and M_{WHP} is the moment contribution from the WHPs (see Figure 3(c)). After decompression of the PT connection (Point 1, see Figure 3(a)), gap opens and the behavior becomes nonlinear elastic with rotational stiffness S_1. At point 2, the upper WHPs yield and M continues to increase with slope S_2. At point 3, the lower WHPs yield and M continues to increase with slope S_3. At point 4, the fuse yields and M continues to increase with slope S_4. When loading is reversed, the connection begins to unload until the gap closes. Equations to calculate $S_{WHP,1}$ to $S_{WHP,3}$, $S_{N,1}$ to $S_{N,2}$, S_1 to S_4 and θ_2 to θ_4 are presented in (Tzimas et al. 2013).

The MWHP-θ is multi-linear elastoplastic. The MWHP-θ curve changes slope two times as the upper WHPs yield at θ_2 and the lower WHPs yield afterwards at θ_3. The M_N-θ curve changes slope at θ_4 when the fuse yields. When loading is reversed and until gap closing, the fuse unloads with its initial stiffness (without yielding in the opposite direction) and the PT bars with their elastic stiffness. This explains why the M_N-θ curve fully unloads with its initial stiffness. Due to residual plastic shortening

of the fuse the length of the PT bars is reduced, so PT bars force when gap closes is lower than the initial post-tensioning force.

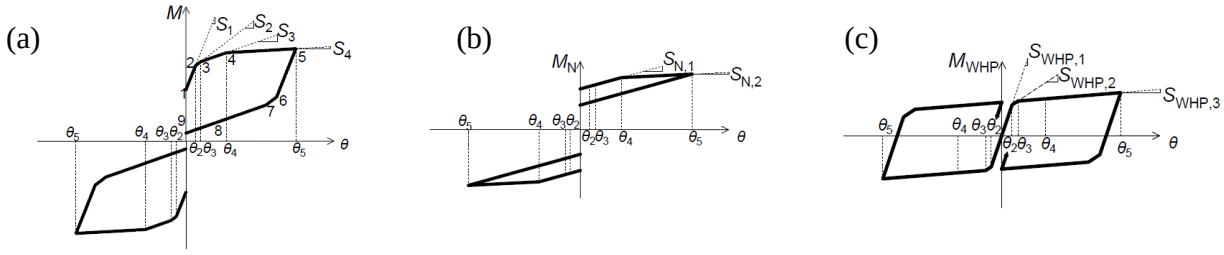

Figure 3. Theoretical cyclic behaviour of the PT connection with WHPs

DESIGN PROCEDURE FOR PT CONNECTIONS WITH WHPs

A new design procedure for PT connections with WHPs has been developed in (Tzimas et al. 2013). Given the PT connections rotations under the DBE and MCE (θ_{DBE} and θ_{MCE}) and the corresponding forces V_{c1u}, V_{c1l} and F_{Dj} from a preliminary pushover analysis of the SC-MRF (Tzimas et al. 2013), the design procedure results in sizing of the connection components (PT bars, WHPs, fuse and reinforcing plates) to achieve a pre-defined target connection performance, and has the following steps:

- *Step (1)*: Calculate the initial post-tensioning force ($T_0=M_d/d_2$) by selecting appropriate values of the ratios $M_{IGO}/M_{pl,b}$ and M_d/M_{IGO}, where M_{IGO} is the moment at point 2 of Figure 3(a) and $M_{pl,b}$ is the beam plastic moment. The first ratio should be less than one to ensure that the SC-MRF will have a base shear strength comparable to that of a conventional moment resisting frame (MRF) and the second ratio should be larger than 0.5 to approximately ensure self centering behaviour of the PT connection.
- *Step (2):* Design the PT bars and the fuse devices by assuming an initial PT bar diameter d_{PT} and calculate the total yield force of the PT bars T_y. By selecting the rotation θ_4 (see Figure 3(a)) associated with yielding of the fuse and by estimating T using equations provided in (Tzimas et al. 2013) as a function of the PT connection rotation, the area of the fuse section equals to $A_{fuse}=T(\theta_4)/f_{y,fuse}$ where $f_{y,fuse}$ is the yield strength of the fuse material. Finally it should be checked if the PT bars yield in a rotation equal to $\gamma_{PT}\cdot\theta_{MCE}$ where γ_{PT} is a safety factor. If that happens design step 2 should be repeated with a larger d_{PT}..
- *Step (3):* Design the WHPs. A complete methodology is presented in (Tzimas et al. 2013).
- *Step (4):* Self-centering capability. The rotation θ_{SC} up to which the PT connection provides Self-centering behaviour is computed using equations presented in (Tzimas et al. 2013)
- *Step (5):* Design the reinforcing plates. The length of the beam flange reinforcing plate, L_{rp}, is designed to control beam flange yielding in the beam for $\theta=\theta_{DBE}$. L_{rp} should satisfy the inequality ($L_{rp}\geq(L_b/2)\cdot(M-M_{rp})/M$) where L_b is the beam clear length and M_{rp} is the moment at the end of the reinforcing plate. M_{rp} is calculated as a function of the beam internal axial force and a predefined target value of $\varepsilon_c/\varepsilon_y$ where ε_c the maximum compressive strain and ε_y the yield strain of the beam material. The

beam internal axial force remains constant due to the slab diaphragm and can be approximately (and conservatively) considered equal to T_0 without considering the column restraint. M depends on the rotation θ and equations based on simple mechanics principles for the computation of M are presented in (Tzimas et al. 2013). The minimum reinforcing plate area, A_{rp}, is calculated based on the assumption that the contact force C_F is applied on the beam's flange and the beam's reinforcing plate. Equations for the computation of the A_{rp} and C_F are provided in (Tzimas et al. 2013).

CONCEPT OF VISCOUS DAMPERS IN PARALLEL OF SC-MRFs

SC-MRFs delay damage in beams and eliminate residual drifts instead of conventional MRFs which are designed to develop plastic hinges at the ends of the beams under the DBE. But both of these systems have same cross sections and so similar steel weight, strength and stiffness (Dimopoulos et al. 2013). For this reason both have comparable peak storey drifts under the DBE and so comparable non-structural damage. Also both frames experience inelastic deformations at the columns bases (Dimopoulos et al. 2013). In this work a design strategy which combines SC-MRFs with viscous dampers is presented. Different design cases of a prototype building consisting of SC-MRFs with or without viscous dampers are considered to investigate all possible scenarios, i.e. use of dampers to achieve drifts lower than the EC8 one; to reduce steel weight without exceeding the EC8 drift; or to reduce steel weight and achieve drifts lower than the EC8 one.

PROTOTYPE BUILDING

Figure 4(a) shows the plan view of the 5-storey, 5-bay by 3-bay prototype office building used for the study. The building has two identical perimeter lateral load resisting frames in the longitudinal plan direction. The study focuses on one of these frames, which is designed as steel SC-MRF with or without viscous dampers using the design procedure proposed in (Tzimas et al. 2013). Viscous dampers are inserted in the interior gravity frames (with pin connections) of the building and are coupled with the perimeter frame through the floor diaphragm to form the SC-MRF with viscous dampers shown in Figure 4(b).

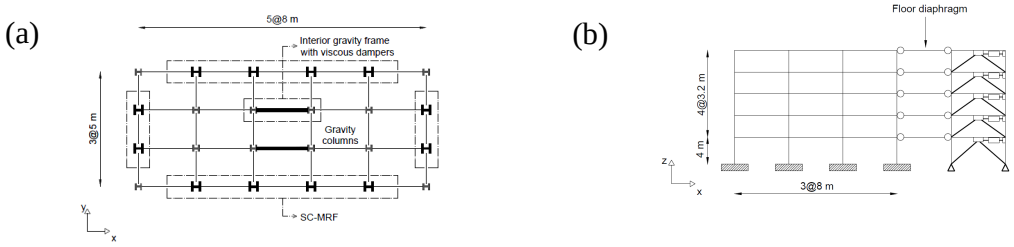

Figure 4. (a) Plan and (b) elevation of the prototype building

DESIGN CASES

Different SC-MRFs are designed using the step-by-step performance-based seismic design procedure of (Tzimas et al. 2013) to investigate all possible design scenarios, i.e. use of dampers to achieve significantly lower peak storey drifts ($\theta_{s\text{-}max}$) than the limit of EC8; to significantly reduce steel weight without exceeding the $\theta_{s\text{-}max}$ limit of EC8; or to reduce steel weight and achieve $\theta_{s\text{-}max}$ lower than the limit of EC8. The PT connections of all the SC-MRFs are designed for $M_{IGO}/M_{pl,b}$=0.65 and M_d/M_{IGO}=0.6. To ensure structural and non-structural damage harmonization, stricter design criteria ($\varepsilon_c/\varepsilon_y$, γ_{PT} and θ_4) are adopted for the PT connections of the SC-MRFs designed for lower $\theta_{s\text{-}max}$. Table 1 provides a direct comparison of the design criteria, steel weight, fundamental period of vibration, T_1, and supplemental damping of the SC-MRFs using viscous dampers. The names of the SC-MRFs, considered in this study are shown in the first column of Table 1. The names notation has the following meaning. CP stands for conventional performance SC-MRFs. These frames are designed to achieve $\theta_{s\text{-}max}$ equal to the EC8 one. HP stands for high performance SC-MRFs, which are designed to achieve $\theta_{s\text{-}max}$, lower than the EC8 one. The number in front of D denoted the damping percentage of the SC-MRF using viscous dampers or by the steel on its own, as in case of CP3D100W (3% of damping due to steel). The number in front of W corresponds to the weight ratio compared to EC8 proposed design. For instance CP22D70W means that this frame is designed with 70% of steel weight, compared to the design results following EC8.

Table 1. Design properties of the SC-MRFs

SC-MRF	Steel weight* (kN)	T_1 (s.)	$\varepsilon_c/\varepsilon_y$	ξ_t (%)	$\theta_{s\text{-}max}$ FOE (%)	$\theta_{s\text{-}max}$ DBE (%)	γ_{PT}	θ_4 fuse activation	$M_{IGO}/M_{pl,b}$	M_d/M_{IGO}
CP3D100W	268	1.27	2.0	3	0.72	1.80	2.1	θ_{DBE}**	0.65	0.60
CP11D86W	230	1.63	2.0	11	0.72	1.80	2.1	θ_{DBE}	0.65	0.60
CP22D70W	190	2.22	2.0	22	0.72	1.80	2.1	θ_{DBE}	0.65	0.60
HP19.5D86W	230	1.63	1.3	19.5	0.60	1.50	2.6	$1.2\theta_{DBE}$	0.65	0.60
HP20D100W	268	1.27	1.0	20	0.48	1.20	3.5	$1.5\theta_{DBE}$	0.65	0.60

MODELLING IN OPENSEES

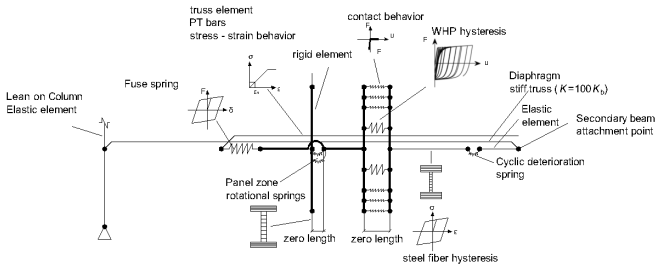

Figure 5. Model for an exterior PT connection with WHPs and associated beams and columns

A simplified numerical model for PT connections with WHPs (see Figure 5) has been developed in OpenSees (Dimopoulos et al. 2013, Tzimas et al. 2013). In this model the PT connections and the associated beams and columns, consist of nonlinear beam-column elements, and hysteretic and contact zero-length uniaxial elements,

appropriately placed into the beam-column interface (see Figure 5). Further details of the model are provided in (Dimopoulos et al. 2013, Tzimas et al. 2013).

PUSHOVER ANALYSES

Numerical models of the five SC-MRFs presented in Table.1 have been developed according to the proposed modelling (Dimopoulos et al. 2013, Tzimas et al. 2013). Monotonic pushover analyses up to 10% roof drift (θ_r) and cyclic pushover analyses up to the DBE roof drift for all five design cases have been conducted.

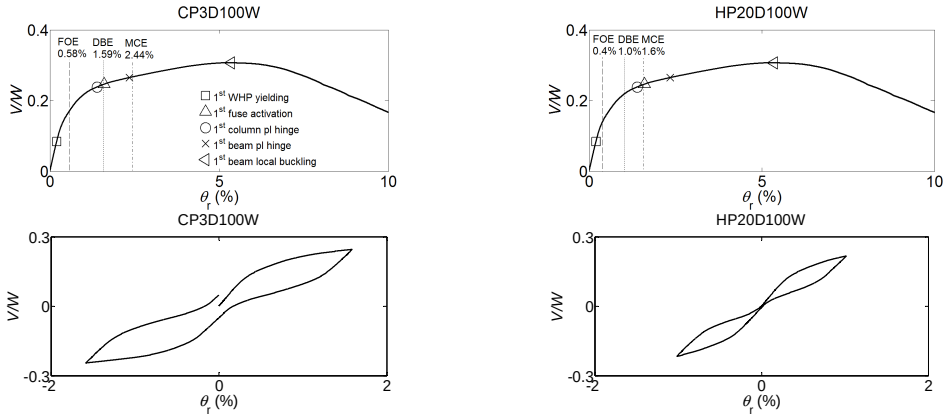

Figure 6. Monotonic and cyclic pushover curves of CP3D100W and HP20D100W

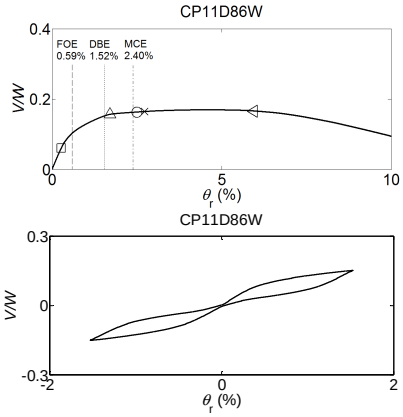

Figure 7. Monotonic and cyclic pushover curve of CP11D86W

Additional damping results in lower drifts under the same seismic intensities and so more effective structural and non-structural performance. Figure 6 shows that HP20D100W frame eliminates residual drifts under the DBE compared to CP3D100W frame.

In SC-MRFs with lower steel weight, the development of the column plastic hinge occurs in higher drifts than in those with higher steel weight, so residual drifts are reduced. Figure 7 shows that CP11D86W has eliminated residual drifts instead of CP3D100W (see Figure 6).

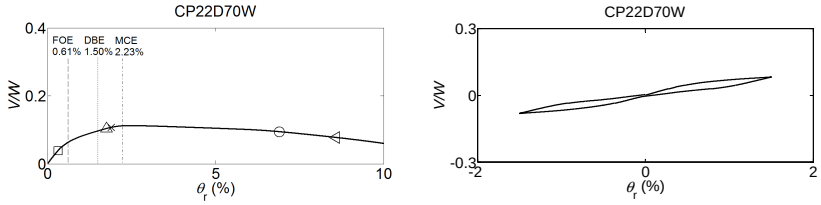

Figure 8. Monotonic and cyclic pushover curve of CP22D70W

The decay in the pushover curves denotes static collapse of the structure and occurs at θ_r higher than 5% due to beam local buckling in all the cases except from the CP22D70W in which occurs due to P-Δ effects at columns (see Figure 8).

FRAGILITY CURVES – COLLAPSE RESISTANCE

Dynamic nonlinear analyses have been conducted to evaluate the seismic performance of all design cases. The ground motions were scaled to the DBE, MCE and 2MCE seismic intensities. Having the peak storey drifts ($\theta_{s,max}$) and residual drifts ($\theta_{s,res}$) for all the SC-MRFs after the dynamic analyses, fragility curves are constructed and the probability of collapse under 2MCE seismic intensity is obtained.

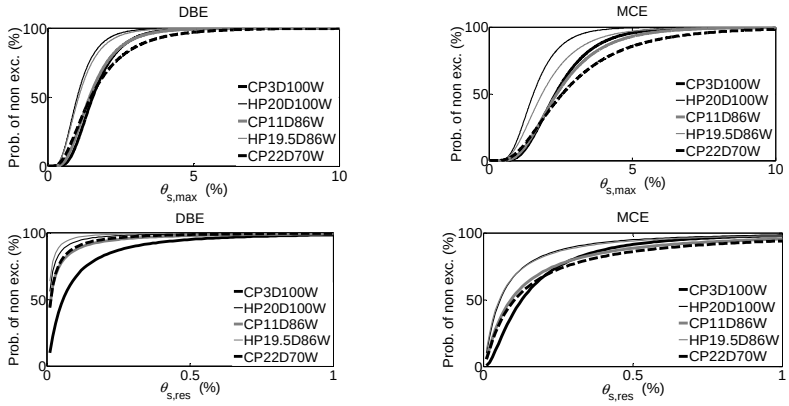

Figure 9. Fragility curves of $\theta_{s,res}$ and $\theta_{s,max}$ under DBE and MCE

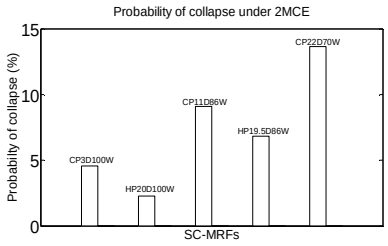

Figure 10. Probability of collapse under 2MCE

Figure 9 shows the $\theta_{s,max}$ and $\theta_{s,res}$ fragility curves of the SC-MRFs under the DBE and MCE. High Performance (HP) SC-MRFs have significantly better performance with $\theta_{s,max}$ and $\theta_{s,res}$ fragility curves clearly shifted to the left. This demonstrates the effectiveness of supplemental damping to improve the structural and

non-structural performance of SC-MRFs. All Conventional Performance (CP) SC-MRFs have almost identical performance, apart from probabilities of non-exceedance higher than 70% under DBE and 50% under MCE for which CP22D70W has a worse performance. This demonstrates that steel SC-MRFs with viscous dampers can be designed for less steel weight without compromising their performance. But a restriction on the strength reduction may need to be established before allowing such a design philosophy in future versions of seismic codes.

None of the SC-MRFs becomes globally unstable (i.e. show unbounded response) under the MCE ground motions. All the SC-MRFs collapsed under a few ground motions from the analyses conducted under the 2MCE seismic intensities. The probability of collapse for each SC-MRF under 2MCE is appeared in Figure 10. At this point it should be noted that these results show that the proposed designs over-qualify the minimum requirements of (FEMA. 2008), which sets a limit on the maximum permissible MCE probability of collapse equal to 10%.

CONCLUSIONS

In this paper a new design procedure for PT connections using a fuse-PT bar system and WHPs has been developed. A design strategy combining steel SC-MRFs with viscous dampers is also presented. Different designs of the SC-MRF with or without viscous dampers and reduced weight of steel were considered for a prototype building. Nonlinear pushover and dynamic analyses of all design cases were conducted using models capable to capture all possible structural limit states up to collapse. Analyses results show that supplemental damping reduces the peak storey and residual drifts of SC-MRFs under DBE and MCE so improves the structural and non-structural behaviour. Design cases with viscous dampers and lighter weight of steel delay the damage at the columns bases, so reduce residual drifts. Analyses results demonstrate that steel SC-MRFs with viscous dampers can be designed for less steel weight without compromising their performance. But a restriction on the strength reduction may need to be established before allowing such a design philosophy in future versions of seismic codes. The probability of collapse under 2MCE seismic intensities is low for all of the SC-MRFs while none of them collapsed under MCE.

ACKNOWLEDGEMENT

Financial support for this work is provided by the Engineering and Physical Sciences Research Council of the United Kingdom; Grant Ref: EP/K006118/1

REFERECNCES

Dimopoulos AI, Karavasilis TL, Vasdravellis G, Uy B. Seismic design, modelling and assessment of self-centering steel frames using post-tensioned connections with web hourglass shape pins. Bulletin of Earthquake Engineering 2013; in press.

EC8. Eurocode 8. Design of structures for earthquake resistance. 2008.

FEMA P695. Quantification of building seismic performance factors. ATC-63 Project. Applied Technology Council. CA. USA, 2008.

Garlock M, Sause R, Ricles JM. Behavior and design of posttensioned steel frame systems. Journal of Structural Engineering 2007; 133(3): 389-399.

Kim HJ, Christopoulos C. Seismic design procedure and seismic response of post-tensioned self-centering steel frames. Earthquake Engineering and Structural Dynamics 2008; 38(3): 355-376.

Symans MD, Charney FA, Whittaker AS, Constantinou MC, Kircher CA, Johnson MW, McNamara RJ. Energy dissipation systems for seismic applications: current practice and recent developments. Journal of Structural Engineering 2008; 134(1): 3-21.

Tzimas AS, Dimopoulos AI, Karavasilis TL. Self-centering steel frames with fuse-post-tensioned bars and viscous dampers: seismic design procedure, fragilities and collapse resistance. Earthquake Engineering and Structural Dynamics 2013; under review.

Vasdravellis G, Karavasilis TL, Uy B. Large-scale experimental validation of steel post-tensioned connections with web hourglass pins. Journal of Structural Engineering (ASCE) 2013; 139(6):1033-1042.

Vasdravellis G, Karavasilis TL, Uy B. Finite element models and cyclic behaviour of self-centering post-tensioned connections with web hourglass pins. Engineering Structures 2013; 52:1-16.

KEYWORDS

Self-centering; Post-tensioned; Seismic design; Collapse; Steel MRFs; Eurocode 8